On the sensitivity of P-wave receiver functions to seismometer orientation

Diogo Farrapo Albuquerque[1], Marcelo Peres Rocha[1], George Sand França[1] and Reinhardt A. Fuck[2].
[1]Seismological Observatory (SIS-UnB); [2]Institute of Geosciences (IG-UnB).

Abstract

The Receiver Function technique relies on the correct rotation of three-component seismograms to isolate the Earth's seismic velocity structure beneath a receiver. The right rotation procedure depends on the correct orientation of the seismometer of the station. Based on that fact, we analyzed the influence of seismometer orientation on the amplitude of the main Receiver Function phases used to estimate crustal thickness and V_P/V_S. The influence of the orientation error on this technique was confirmed by the amplitude reduction of P and P_S phases, which indicated a threshold of 85º (P_S) as the maximum orientation error for Receiver Functions studies. The estimates of crustal thickness and V_P/V_S were more strongly influenced by orientation errors equal or larger than 85º. This suggests that crustal thickness and V_P/V_S estimated by previous studies are reliable even for stations with large orientation errors. Also, the variation in P and P_S amplitudes indicate that Receiver Functions can be used as a tool to estimate seismometer orientation.

Introduction

Receiver Function (RF) is a straightforward technique extensively used to map seismic discontinuities and estimate the ratio between P and S-wave velocities (V_P/V_S). This technique relies on the correct rotation of three-component seismograms, which are used to isolate the seismic velocity structure, beneath a receiver (station), by deconvolving the vertical from the rotated horizontal components (Langston, 1979; Ammon, 1991; Zandt and Ammon, 1995).

In Brazil, many relevant studies have employed RF to infer the crustal velocity structure of the main structural provinces: Amazonian Craton (Rosa et al., 2016; Albuquerque et al., 2017); Borborema Province (Pavão et al., 2013; Luz et al., 2015; Fianco et al., 2019); Paraná Basin (Julià et al., 2008; Zevallos et al., 2009; Rivadeneyra-Vera et al., 2019); Pantanal Province (Cedraz et al., 2020); Tocantins Province (Trindade et al., 2014; Albuquerque et al., 2017); São Francisco Craton and Mantiqueira Province (Assumpção et al., 2004; França and Assumpçao, 2004); Parecis Basin (Barros and Assumpção, 2011; Albuquerque et al., 2017) and Parnaíba Basin (Coelho et al., 2018).

A substantial part of the published studies used data from the Brazilian Seismographic Network (RSBR), which has some misoriented stations identified by Bianchi (2015) and Albuquerque (2017). Except for the latter study, which applied an azimuth correction based on the estimated orientation error estimated, there is no indication that previous studies analyzed the orientation of the seismometers or applied any azimuth correction to estimate crustal thickness and V_P/V_S.

Therefore, considering that the RF relies on the correct rotation of three-component seismograms, the existence of misoriented stations in RSBR and the number of papers published using the RF technique, this study aims to investigate the sensitivity of the seismometer orientation on the calculation of RF waveforms used to estimate crustal thickness and V_P/V_S.

Data

We used data recorded by BOAV, a RSBR broadband station deployed in Roraima, Brazil (Figure 1). This station was selected because it has the largest confirmed orientation error identified in RSBR during field maintenance (Albuquerque et al., 2023; under review).

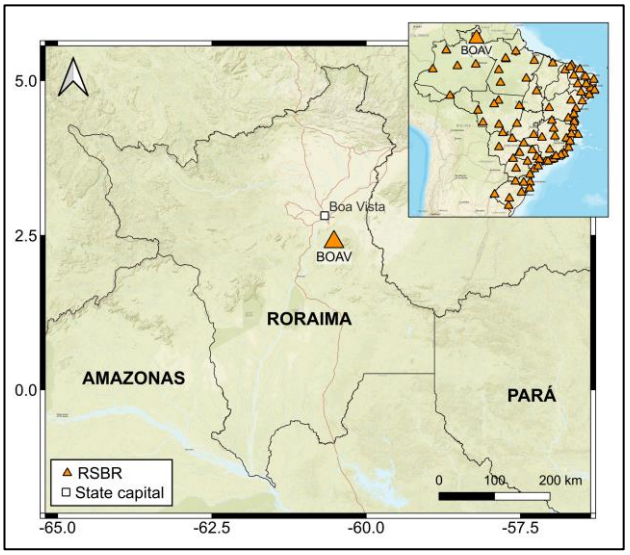

Figure 1 – Location of BOAV and all the RSBR stations (inset in the upper right corner).

The BOAV station was deployed on Jan 24th, 2014, with the North-South component of the seismometer inverted, producing an orientation error of 180º (Figure 2). On Nov 29th, 2016, the seismometer orientation was corrected. Since the orientation error was identified and confirmed with a magnetic compass in the field, BOAV is suitable to

investigate the possible influence of the orientation error on RF.

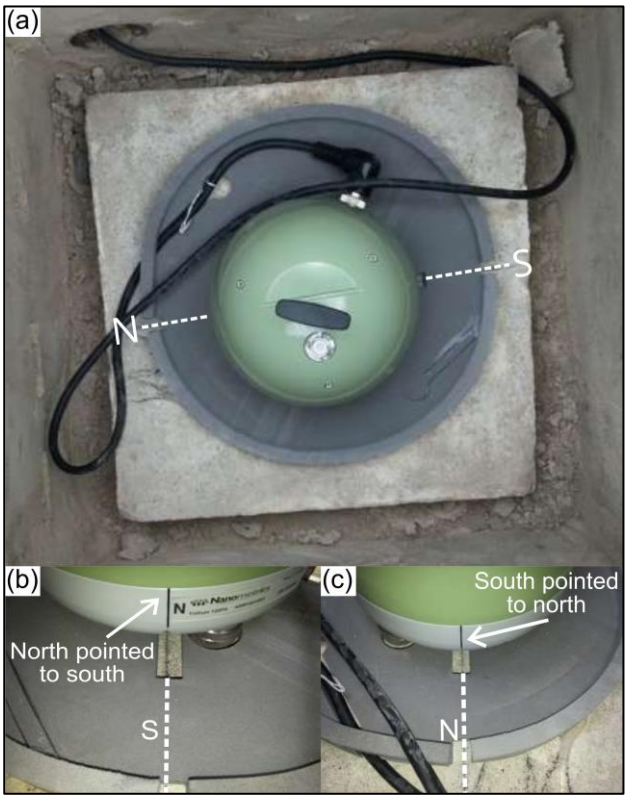

Figure 2 – Nanometrics Trillium 120PA broadband seismometer deployed at BOAV station. (a) Indication of the geographic north (N) and south (S). (b) Indication that the north of the seismometer was pointed to the south. (c) Indication that the south of the seismometer was pointed to the north.

We used data from Jan 24th, 2014, to Dec. 29th, 2019. Two criteria were considered in the event selection: epicentral distance (Δ) and magnitude (M). We selected events with 30º ≤ Δ ≤ 95º and M ≥ 5.0.

Events with Δ < 30° were not selected due to P-wave triplications in the upper mantle discontinuities (LeFevre and Helmberger, 1989), and Δ > 95º because of the P-wave shadow zone (Shearer, 2009). Events with M < 5.0 were not selected because they tend to have low signal to noise ratio (SNR) caused by attenuation effects. We also removed the linear trend and the mean of all seismograms and visually inspected them to remove signals with low P-wave SNR and gaps inside a time window including 5 s before and 30 s after P-arrival.

Figure 3 shows the epicenter of each teleseismic event, the directional histogram indicating the azimuth of the P-wave arrival at the station (back azimuth) and the histograms of epicentral distance, back azimuth, event depth and magnitude.

Most of the teleseismic events were located in the West coast of the United States, Central America, Chile and near the South Sandwich Islands (Figure 3a). This causes a concentration of epicentral distances between 30º and 42º as well as between 60º and 68º (Figure 3c). In terms of back azimuth, there is also concentration from 160º to 190º, from 210º to 230º, and from 280º to 330º (Figure 3b, d). Most of the events occurred at depths ranging from 20 km to 80 km (Figure 3e) and magnitudes from 5.0 to 7.0 (Figure 3f).

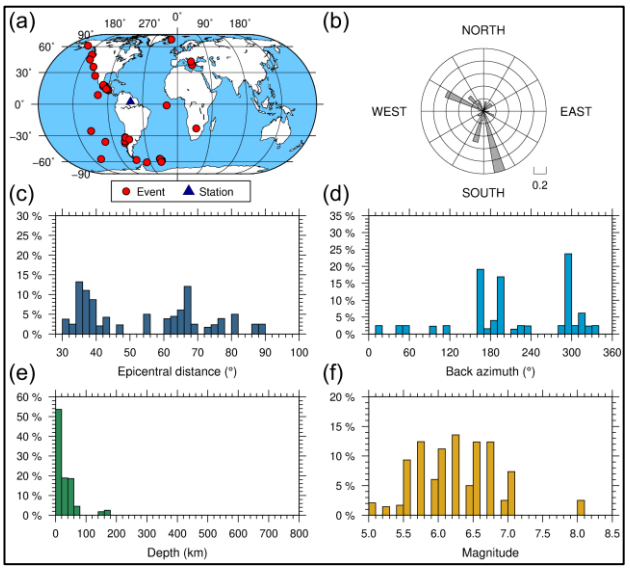

Figure 3 – (a) Location of the teleseismic events. (b) Directional histogram indicating the back azimuth. (c) Histogram of epicentral distance. (d) Histogram of back azimuth. (e) Histogram of event depth. (f) Histogram of event magnitude.

Method

The RF technique is based on the principle that a teleseismic P-wave, incident at the base of the crust, generates P to S converted phases (P_S) and multiple converted phases within the crust (PpP_S and $PpS_S+P_SP_S$). Assuming a horizontally or radially stratified earth structure, the amplitudes of the arrivals in RF traces depend on the velocity contrast between mantle and crust, and the incidence angle of the P-wave (ray parameter). The arrival times of Ps and multiples depend on the crustal thickness, the crustal velocities of P (V_P) and S (V_S) and the P-wave incidence angle (Langston, 1979; Ammon, 1991; Zandt and Ammon, 1995).

Through the deconvolution of the vertical component from the radial, the structure near the receiver (station) is isolated from the source and distant structure effects. The deconvolution generates time series similar to seismograms, with typical peaks and troughs indicating the direct P-wave, the converted P_S and multiples converted phases (Langston, 1979; Ammon, 1991; Zandt and Ammon, 1995).

Since there is an abrupt change in seismic velocities and densities at the Moho discontinuity, P_S-wave is often the highest peak following the direct P. Therefore, the arrival time of P-P_S-waves and multiples can be used to estimate crustal thickness and V_P/V_S, given the average crustal velocities (Zhu and Kanamori, 2000).

The Iterative Time Domain Deconvolution (ITERDECON) was used to generate the RF traces. It is a fast forward algorithm developed by Ligorría and Ammon (1999). This

algorithm is based on the least-squares minimization of the difference between the observed horizontal seismogram and a predicted signal. This signal is generated by the convolution of an iteratively updated spike train with the vertical-component seismogram to reproduce the radial and tangential seismograms.

The input parameters for ITERDECON were: 2.5 for the Gaussian filter, 80% for the minimum reproduction of radial traces during deconvolution and 200 iterations for the RF calculation.

According to Langston (1979), the Gaussian filter was chosen because of its simple shape, zero phase distortion, and lack of side-lobes. This filter allowed us to remove high frequency noise or frequencies not related to the P, P_S and multiples phases.

The percentage of the radial seismogram that is reproduced by the predicted signal generated by the ITERDECON algorithm can be used as quality parameter. This parameter allows the removal of a substantial number of RF traces with high noise levels. The number of iterations (200) was chosen based on the maximum permitted by ITERDECON algorithm.

The H-k stacking method (Zhu and Kanamori, 2000) was used to estimate the crustal thickness (H) and V_P/V_S (k). This method stacks radial RF traces on the predicted arrival times of P_S and multiples, and the best result is reached when all the three phases are stacked coherently (maximum in the H-k function). H-k also demands, as a priori information, the average V_P in the crust and three weighting factors, one for each phase (w1, w2 and w3).

We used a V_P of 6.4 km/s, which corresponds to the average crustal velocity of P-waves in the Amazonian Craton (Albuquerque et al., 2017), where BOAV was installed. The standard values were used for the weighting factors, as suggested by Zhu and Kanamori (2000): w1=0.7, w2=0.2 and w3=0.1. The largest weighting factor was set for P_S, which is the phase with the largest amplitude after the direct P.

Results

In order to investigate the sensitivity of the orientation on RF traces, we selected an event with impulsive P-wave arrival and 90% of reproduction of radial waveform (Figure 4) after correctly orienting the seismometer in the field. We chose a seismogram of the event occurred at 16:14:13.090 (Origin time UTC) on Feb 1st, 2019, near the border between Guatemala and Mexico. This event had a magnitude of 6.2 m_W and depth of 62 km.

The horizontal components of the seismogram in Figure 4 were rotated, from 0º to 180º, adding an orientation error in steps of 5º. Then, the radial RF trace was computed for each step (Figure 5a).

In general, the amplitudes of P (0 s), P_S (~5.1 s), PpP_S (~17.9 s) and PpS_S+PsP_S (~24.5 s) decreased and eventually had its polarity inverted as the orientation error increased (Figure 5a). The P-wave amplitude decreased gradually until inverted when the orientation error reaches 100º. This is corroborated by the chart in Figure 5b, which indicates a P error threshold at 95º, when the amplitude is close to zero.

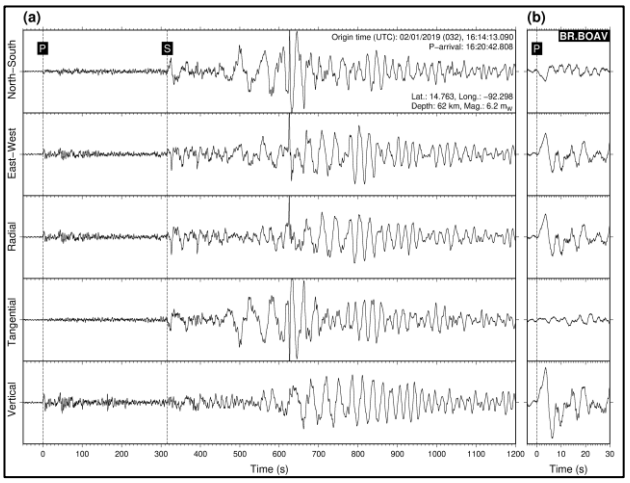

Figure 4 – (a) Seismograms of the earthquake occurred near the border between Guatemala and Mexico. The origin parameters are indicated in the upper right. North-South, East-West and Vertical are the original components of the seismogram recorded by the BOAV station. Radial and Tangential are the rotated components. The arrivals of P and S waves are highlighted in black. (b) Time window indicating the zoomed P-wave arrival.

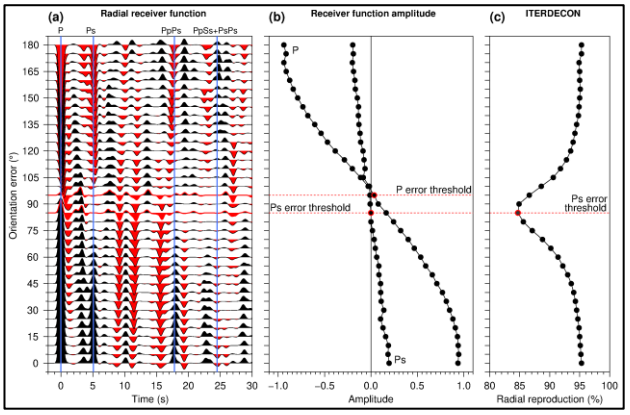

Figure 5 – (a) Radial receiver functions computed for each 5º increasing in the orientation error. The vertical blue lines indicate the phases: P (0 s), P_S (~5.1 s), PpP_S (~17.9 s) and $PpS_S+P_SP_S$ (~24.5 s). (b) P and P_S amplitude variation for each 5º increasing in the orientation error. The dotted red lines and the highlighted circles indicate the threshold of orientation error considering P and Ps amplitudes. (c) Percentage of reproduction of the radial component computed by the Iterative Time Domain Deconvolution (ITERDECON). The highlighted circle and the dotted red line indicate the minimum percentage reproduction of the radial.

The amplitude of Ps decreased gradually until it reached zero, when the orientation error was equal to 85º, and its polarity inverted at 90º. This is corroborated by the chart in Figure 5b, which indicates the Ps error threshold (red dotted lines). The same occurred to the PpP_S, but its amplitude reached zero at 105º. The $PpS_S+P_SP_S$ amplitude increased until 95º and became positive between 100º and 105º.

The reproduction of the radial component computed by ITERDECON (Figure 5c) was also affected by the

increasing orientation error. The reproduction reached a minimum of about 85%, when the orientation error is 85º, and increased again after that. The minimum amplitude of P_S coincided with the minimum reproduction of the radial component (Figure 5b, c).

Based on the available information about the crustal thickness in the region near the BOAV station, the arrival time of the P_S-wave converted at Moho is expected to be between 4 and 5 seconds (Albuquerque et al., 2017), thus phases arriving before that interval are possibly related to crustal discontinuities. The phase between P and P_S, at about 3.8 seconds (Figure 5a), is possibly a conversion caused by the upper to lower crust interface (Conrad discontinuity) (Kearey et al., 2009).

Since the velocity contrast between lower and upper crust (5.8 to 6.5 km/s) is smaller than between mantle and crust (6.5 to 8.0 km/s) (Kennett and Engdahl, 1991), we expect RF traces with P_S converted at Conrad discontinuity to have smaller amplitude than P_S at Moho. Therefore, when the Moho P_S amplitude is smaller than Conrad P_S (Figure 5a, error orientation of about 60º), this may indicate that the seismometer is misoriented. Additionally, the time of P_S converted at Conrad seems to change as the error in orientation changes, or at least the shape of the related pulse, which can introduce errors in estimating this discontinuity.

The example illustrated in Figure 5 is close to an ideal case since the event has a high SNR and produced a RF trace with the main phases easily identifiable. However, the real case can be quite different from that example.

To have a better understanding of the amplitude behavior of the main phases, we selected 45 RF traces with discernible P and P_S phases, and reproduction percentage larger than 80% considering the case with no orientation error (after the seismometer was reoriented in the field). Then, the RF traces were calculated adding 5º in the orientation error until it reached 180º. The maximum amplitude of P and P_S were measured, and their mean values were estimated as well as their reproduction percentage (Figure 6).

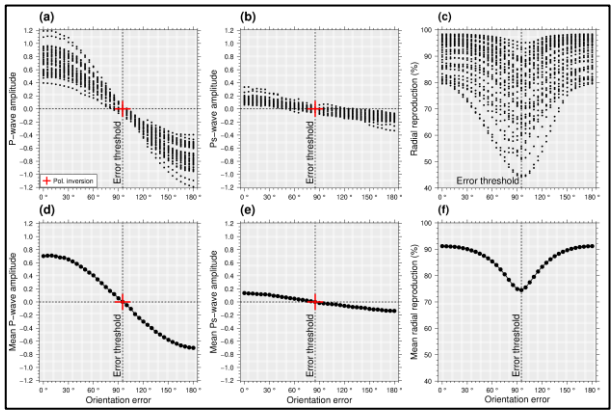

Figure 6 – Relation between orientation error and amplitudes of (a) P-wave and (b) Ps-wave. (c) Relation between orientation error and reproduction of the radial component. Relation between orientation error and mean amplitude of (d) P-wave and (e) Ps-wave. (f) Relation between orientation error and mean reproduction of the radial component. The dotted lines and crosses point out the orientation error threshold.

The influence of orientation errors on P and P_S amplitudes can be observed in Figure 6. The amplitudes of the P and P_S-waves reached zero when the errors were equal to 95º and 85º, respectively (Figure 6a, b). We also observed that the mean amplitudes indicate that effect more clearly and the amplitudes of P and P_S inverted when the orientation errors were larger than those values (Figure 6d, e). Therefore, we can reassert that stations with orientation errors greater than 85º cannot be used without an orientation correction for RF studies, because it is hardly possible to estimate crustal thickness and V_P/V_S when P_S amplitude is zero or close to it. Although the 85º threshold seems high, it is only a reference for the maximum orientation error to consider the data useless for RF technique. However, it is necessary to be careful when analyzing and interpreting the estimates for data with orientation errors below that threshold, especially for seismic anisotropy studies.

Compared to the reproduction percentage of the radial seismogram (Figure 6c, f), the orientation error threshold is different from the one in Figure 5c (85º). The reproduction reached the lowest value when the orientation error was equal to 95º, which coincides with the P-wave error threshold. Then, the maximum orientation error of which receiver functions are not useful to estimate crustal thickness and V_P/V_S is when the orientation error is 85º (P_S amplitude close to zero).

In order to estimate the H and k for the BOAV station, considering the case of no orientation error (Figure 7), we used H-k stacking (Zhu and Kanamori, 2000) for the same events and RF traces used in Figure 6. The RF traces are sorted by back azimuth in Figure 7a. The H-k stacking result is presented in Figure 7b.

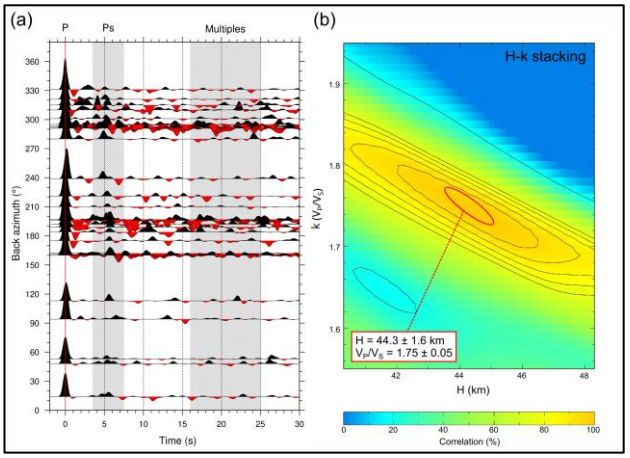

Figure 7 – RF traces generated considering no orientation error. (a) Radial RF traces sorted by back azimuth. The vertical red line indicates the arrival of the direct P-wave and the hatched areas indicate the arrival of P_S and multiples (PpS_S and $PpS_SP_SP_S$). (b) Result of H-k stacking using RF traces computed from 45 events recorded by the BOAV station (same data set used in Figure 6). The crustal thickness (H) and k (V_P/V_S) are indicated in the inset on the left bottom corner. The red ellipse indicates H and k parameter variation. The correlation between H and k is given by the color scale at the bottom.

We estimated an H of 44.3±1.6 km and k equal to 1.75±0.05 (Figure 7b). The estimated H is typical of shields and platforms (Christensen and Mooney, 1995) and V_P/V_S

is typical of felsic crust (Musacchio et al., 1997). The crustal thickness is consistent with recent studies (Albuquerque et al., 2017) and the updated crustal thickness model obtained by Rivadeneyra-Vera et al. (2019).

To evaluate the effects of the station orientation on H and k, we increased the orientation error in steps of 5º (Figure 8). The estimates of H and k are more strongly influenced by orientation errors equal or larger than 85º, when an abrupt change in the estimates occurs (red square, Figure 8a, b). This result corroborates the threshold defined by analyzing the amplitude decay of P_S-wave in the receiver functions directly (Figures 5 and 6).

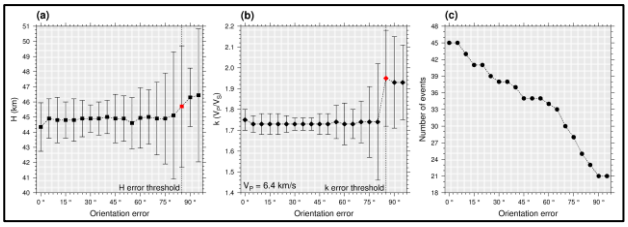

Figure 8 – (a) Crustal thickness (H) estimated by H-k stacking, using RF traces computed from 45 events recorded by BOAV station, for each 5º increment on orientation error. (b) k (V_P/V_S) estimated by H-k stacking for each 5º increment on the orientation error. (c) Number of events for each 5º increment on orientation error. The error bars represent the standard deviation of H and k. The highlighted symbol in red indicates the orientation error threshold for each parameter.

The number of events, with reproduction of the radial component greater than 80%, decreased for each step of 5º in the orientation error (Figure 8c). This occurred because the orientation error has strong influence on the deconvolution, as seen in Figures 5 and 6. Nevertheless, H and k had no remarkable change as the number of events decreased, but the standard deviations tended to increase (error bars in Figure 8a, b), suggesting that the uncertainty increases with the decreasing number of events or increasing the orientation error.

The RF traces and consequently the H-k estimates are not sensitive to orientation errors smaller than 85º. The amplitude of P and P_S are close to the point where the radial becomes the tangential component (90º). This suggests that crustal thickness and V_P/V_S estimated by previous studies can be considered reliable even for stations with large orientation errors. However, if the objective is to estimate Conrad depth, orientation errors smaller than 85º could influence the estimates.

Since the amplitude of P and P_S decreases gradually with the increasing orientation error, the RF traces could be used as a tool to analyze the orientation error of seismometers. Therefore, it expected that the maximum of P and P_S amplitudes will be reached when the error is close to zero.

Conclusions

The influence of the orientation error on RF technique was confirmed by the amplitude reduction of P and P_S phases, which indicate a threshold of 85º (P_S) as the maximum orientation error to consider the station not suitable for RF. Also, the estimates of crustal thickness and V_P/V_S were more strongly influenced by orientation errors equal or larger than 85º.

The RF traces and consequently the crustal thickness and V_P/V_S estimates were not sensitive to orientation errors smaller than 85º. The amplitude of P and P_S were close to the point where the radial becomes the tangential component (90º). This suggests that crustal thickness and V_P/V_S estimated by previous studies are reliable even for stations with large orientation errors.

The arrival of the P_S phase converted at the upper to lower crust interface (Conrad discontinuity) changes as the orientation error increases, making it possible that Conrad depth estimates could be wrong for orientation errors smaller than 85º. Also, if the amplitude of the P_S related to Conrad discontinuity is larger than the P_S at Moho, it is a sign that the seismometer of the station could be misoriented.

Since maximum P and P_S amplitudes will be reached when the error is close to zero, the analysis of P and P_S amplitudes can be used as a tool to estimate seismometer orientation error.

Acknowledgments

This study was financed in part by the Coordenação de Aperfeiçoamento de Pessoal de Nível Superior - Brazil (CAPES) - Finance Code 001. We thank Petrobras and the Brazilian Geological Survey (CPRM) for funding the Brazilian Seismographic Network (RSBR). Support from INCT Estudos Tectônicos (CNPq, CAPES, FAPDF) is acknowledged. We thank the Conselho Nacional de Desenvolvimento Científico e Tecnológico (CNPq) for the research fellowship grants 315613/2021-1 (M. P. Rocha), 310240/2020-4 (G. S. França) and 30.2885/2021-8 (R. A. Fuck). We also would like to thank the Seismological Observatory of University of Brasília (SIS-UnB) for all its scientific importance for the Brazilian seismological community.

References

Albuquerque, D. F., 2017, Estudos Crustais nas Regiões Norte e Centro-Oeste do Brasil, Dissertação de mestrado, Universidade de Brasília, Brasília.

Albuquerque, D. F., G. S. França, L. P. Moreira, M. Assumpção, M. Bianchi, L. V. Barros, C. C. Quispe, and M. E. Oliveira, 2017, Crustal structure of the Amazonian Craton and adjacent provinces in Brazil, J South Am Earth Sci, 79, 431–442, doi: 10.1016/j.jsames.2017.08.019.

Albuquerque, D. F., M. Peres Rocha, M. Ianniruberto, G. S. França, R. A. Fuck, M. Figueredo, and M. B. Aguiar, 2023, Estimating seismometer component orientation of the Brazilian Seismographic Network using teleseismic P-wave particle motion analysis and directional statistics, Bulletin of the Seismological Society of America.

Ammon, C. J., 1991, The isolation of receiver effects from teleseismic P waveforms, Bulletin - Seismological Society of America, 81, no. 6, 2504–2510.

Assumpção, M., M. An, M. Bianchi, G. S. L. França, M. Rocha, J. R. Barbosa, and J. Berrocal, 2004, Seismic studies of the Brasília fold belt at the western border of the São Francisco Craton, Central Brazil, using receiver function, surface-wave dispersion and teleseismic tomography, Tectonophysics, 388, nos. 1–4, 173–185, doi: 10.1016/j.tecto.2004.04.029.

Barros, L. V., and M. Assumpção, 2011, Basement depths in the Parecis Basin (Amazon) with receiver functions from small local earthquakes in the Porto dos Gaúchos seismic zone, J South Am Earth Sci, 32, no. 2, 142–151, doi: 10.1016/j.jsames.2011.04.002.

Bianchi, M., 2015, RSBR automatic sensor orientation analysis by P-wave incidence direction, in *1st Brazilian Symposium on Seismology*, 1–3.

Cedraz, V., J. Julià, and M. Assumpção, 2020, Joint Inversion of Receiver Functions and Surface-Wave Dispersion in the Pantanal Wetlands: Implications for Basin Formation, J Geophys Res Solid Earth, 125, no. 2, 0–3, doi: 10.1029/2019JB018337.

Christensen, N. I., and W. D. Mooney, 1995, Seismic velocity structure and composition of the continental crust: A global view, J Geophys Res Solid Earth, 100, no. B6, 9761–9788, doi: 10.1029/95JB00259.

Coelho, D. L. O., J. Julià, V. Rodríguez-Tribaldos, and N. White, 2018, Deep crustal architecture of the Parnaíba basin of NE Brazil from receiver function analysis: Implications for basin subsidence, Geol Soc Spec Publ, 472, no. 1, 83–99, doi: 10.1144/SP472.8.

Fianco, C. B., G. S. França, D. F. Albuquerque, C. da S. Vilar, and R. M. Argollo, 2019, Using the receiver function for studying earth deep structure in the Southern Borborema Province, J South Am Earth Sci, 94, no. August 2018, 102221, doi: 10.1016/j.jsames.2019.102221.

França, G. S., and M. Assumpçao, 2004, Crustal structure of the Ribeira fold belt, SE Brazil, derived from receiver functions, J South Am Earth Sci, 16, no. 8, 743–758, doi: 10.1016/j.jsames.2003.12.002.

Julià, J., M. Assumpção, and M. P. Rocha, 2008, Deep crustal structure of the Paraná Basin from receiver functions and Rayleigh-wave dispersion: Evidence for a fragmented cratonic root, J Geophys Res Solid Earth, 113, no. B8, 1–23, doi: 10.1029/2007JB005374.

Kearey, P., K. A. Klepeis, and F. J. Vine, 2009, Global Tectonics, Wiley-Blackwell, Chichester.

Kennett, B. L. N., and E. R. Engdahl, 1991, Traveltimes for global earthquake location and phase identification, Geophys J Int, 105, no. 2, 429–465, doi: 10.1111/j.1365-246X.1991.tb06724.x.

Langston, C. A., 1979, Structure under Mount Rainier, Washington, inferred from teleseismic body waves, J Geophys Res, 84, no. B9, 4749, doi: 10.1029/JB084iB09p04749.

LeFevre, L. V., and D. V. Helmberger, 1989, Upper mantle P velocity structure of the Canadian Shield, J Geophys Res, 94, no. B12, 17749, doi: 10.1029/JB094iB12p17749.

Ligorría, J. P., and C. J. Ammon, 1999, Iterative deconvolution and receiver-function estimation, Bulletin of the Seismological Society of America, 89, no. 5, 1395–1400.

Luz, R. M. N., J. Julià, and A. F. do Nascimento, 2015, Crustal structure of the eastern Borborema Province, NE Brazil, from the joint inversion of receiver functions and surface wave dispersion: Implications for plateau uplift, J Geophys Res Solid Earth, 120, no. 5, 3848–3869, doi: 10.1002/2015JB011872.

Musacchio, G., W. D. Mooney, J. H. Luetgert, and N. I. Christensen, 1997, Composition of the crust in the Grenville and Appalachian Provinces of North America inferred from V P /V S ratios, J Geophys Res Solid Earth, 102, no. B7, 15225–15241, doi: 10.1029/96JB03737.

Pavão, C. G., G. S. França, M. Bianchi, T. de Almeida, and M. G. Von Huelsen, 2013, Upper-lower crust thickness of the Borborema Province, NE Brazil, using Receiver Function, J South Am Earth Sci, 42, 242–249, doi: 10.1016/j.jsames.2012.07.003.

Rivadeneyra-Vera, C. et al., 2019, An Updated Crustal Thickness Map of Central South America Based on Receiver Function Measurements in the Region of the Chaco, Pantanal, and Paraná Basins, Southwestern Brazil, J Geophys Res Solid Earth, 124, no. 8, 8491–8505, doi: 10.1029/2018JB016811.

Rosa, João Willy Corrêa, José Wilson Corrêa Rosa, and R. A. Fuck, 2016, The structure of the Amazonian craton: Available geophysical evidence, J South Am Earth Sci, 70, no. May, 162–173, doi: 10.1016/j.jsames.2016.05.006.

Shearer, P. M., 2009, Introduction to Seismology, Cambridge University Press, Cambridge.

Trindade, C. R. da, J. E. P. Soares, R. A. Fuck, A. C. Carmelo, and C. L. O. Peixoto, 2014, Estrutura crustal do Brasil Central, Comunicações Geológicas, 101, no. I, 339–343.

Zandt, G., and C. J. Ammon, 1995, Continental crust composition constrained by measurements of crustal Poisson's ratio, Nature, 374, no. 6518, 152–154, doi: 10.1038/374152a0.

Zevallos, I., M. Assumpção, and A. L. Padilha, 2009, Inversion of teleseismic receiver function and magnetotelluric sounding to determine basement depth in the Paraná Basin, SE Brazil, J Appl Geophy, 68, no. 2, 231–242, doi: 10.1016/j.jappgeo.2008.11.002.

Zhu, L., and H. Kanamori, 2000, Moho depth variation in southern California from teleseismic receiver functions, J Geophys Res Solid Earth, 105, no. B2, 2969–2980, doi: 10.1029/1999JB900322.